A&A 474, 67–76 (2007)
DOI: 10.1051/0004-6361:20077335

Astronomy & Astrophysics

Outflow or galactic wind: the fate of ionized gas in the halos of dwarf galaxies⋆

J. van Eymeren[1], D. J. Bomans[1], K. Weis[1,2], and R.-J. Dettmar[1]

[1] Astronomisches Institut der Ruhr-Universität Bochum, Universitätsstraße 150, 44780 Bochum, Germany
e-mail: jeymeren@astro.ruhr-uni-bochum.de
[2] Lise Meitner Fellowship

Received 21 February 2007 / Accepted 16 August 2007

ABSTRACT

Context. Hα images of star bursting irregular galaxies reveal a large amount of extended ionized gas structures, in some cases at kpc-distance away from any place of current star forming activity. A kinematic analysis of especially the faint structures in the halo of dwarf galaxies allows insights into the properties and the origin of this gas component. This is important for the chemical evolution of galaxies, the enrichment of the intergalactic medium, and for the understanding of the formation of galaxies in the early universe.
Aims. We want to investigate whether the ionized gas detected in two irregular dwarf galaxies (NGC 2366 and NGC 4861) stays gravitationally bound to the host galaxy or can escape from it by becoming a freely flowing wind.
Methods. Very deep Hα images of NGC 2366 and NGC 4861 were obtained to detect and catalog both small and large scale ionized gas structures down to very low surface brightnesses. Subsequently, high-resolution long-slit echelle spectroscopy of the Hα line was performed for a detailed kinematic analysis of the most prominent filaments and shells. To calculate the escape velocity of both galaxies and to compare it with the derived expansion velocities of the detected filaments and shells, we used dark matter halo models.
Results. We detected a huge amount of both small scale (up to a few hundred pc) and large scale (about 1–2 kpc of diameter or length) ionized gas structures on our Hα images. Many of the fainter ones are new detections. The echelle spectra reveal outflows and expanding bubbles/shells with velocities between 20 and 110 km s^{-1}. Several of these structures are in accordance with filaments in the Hα images. A comparison with the escape velocities of the galaxies derived from the NFW dark matter halo model shows that all gas features stay gravitationally bound.

Key words. galaxies: irregular – galaxies: ISM – galaxies: kinematics and dynamics – galaxies: structure

1. Introduction

Irregular dwarf galaxies can be the sites of giant star formation regions. The interplay between massive stars and the interstellar medium (ISM) has a large effect on the formation and the evolution of galaxies. Thereby, dwarf galaxies provide a perfect environment for this interaction as they are simple systems, fragile and hence likely to be strongly affected by both external and internal processes (e.g., Gallagher & Hunter 1984). They generally have low metalicities, which may be a result of their inability to retain newly synthesized metals. Additionally, their surface brightness is very low, which could be due to an expansion of the whole galaxy following the loss of a substantial fraction of its mass or due to the cessation of star formation resulting from the loss of its ISM.

Numerous ionized gas structures up to kpc-size in and around the galactic plane of dwarf galaxies were found (e.g., Bomans et al. 1997; Hunter & Gallagher 1997; Martin 1998; Bomans 2001). These structures can be divided into long, narrow filaments and ring-like structures. Using the definition of Bomans et al. (1997), we refer to all ring-like structures with radii smaller than 500 pc as superbubbles (SB). All ring-like structures larger than 500 pc are called supergiant shells (SGS). Some of these gas features could be the relicts of former shell structures. Others mark the edges of shells that were produced by stellar winds and supernova explosions. Generally, these structures enclose large concentrations of massive stars, so-called OB associations. In this case, the ionization mechanisms are relatively well understood: kinetic energy and momentum are delivered by massive stars to their surroundings through stellar winds and supernova explosions. A hot superbubble then expands into the ISM and sweeps up the ambient gas which forms a thin, dense shell detectable in optical emission line images. Having a sufficiently energetic and long-lasting starburst, this shell can fragment, which allows the gas of the hot bubble to escape.

However, ionized gas structures also exist at kpc-distances away from any place of current star formation or hot massive stars (e.g., Hunter et al. 1993). In this case, the ionization mechanisms are not obvious. Shock waves that are driven by a concentration of massive stars may sweep the interstellar gas out of the star forming region, which leads to the formation of a cavity. Due to lower densities than usual in the ISM, the photons can travel larger distances and can ionize much more distant neutral gas (e.g., Hunter & Gallagher 1997). Apart from photoionization and shock ionization, turbulent mixing layers (Slavin et al. 1993) and magnetic reconnection (Birk et al. 1998) are additional, possible excitation mechanisms.

In theoretical models, the gas, most likely driven by collective supernovae, is expelled into the halos of the galaxies.

⋆ Appendices are only available in electronic form at http://www.aanda.org

Norman & Ikeuchi (1989) developed a theory in which the gas is transported through tunnel-like features into the halo, called chimneys. Depending on the strength of the gravitational potential, the gas may be able to fall back onto the galactic disk, which is described in the galactic fountain scenario (Shapiro & Field 1976).

All these theories are based upon models which try to explain the observations. Several studies also show blowout scenarios by using numerical simulations. Mac Low & Ferrara (1999) developed hydrodynamic models of dwarf galaxies by varying the energy input, the mass of the galaxy and the metallicity. They address analytically and numerically the questions how supernova explosions effect the interstellar medium of dwarf galaxies and what happens to the gas, particularly to the metals. Their simulations show that only in low mass galaxies ($\sim 10^6\,M_\odot$) the probability of gas being able to leave the gravitational potential increases. Silich & Tenorio-Tagle (2001) came to very similar results in their numerical experiments and analytical estimates.

While hunting for ionized gas structures, the vicinity of the Giant Extragalactic H II Regions (GEHR) is of huge interest. GEHRs exceed normal H II regions in size, luminosity and velocity dispersion. Usually, they harbor several concentrations of massive stars. Therefore, a lot of excitation should take place in and around these regions during the lifetime of the OB associations. Our results will show that the presence of excited gas around GEHRs does not necessarily correlate with the age of the OB assocations and is sometimes not limited to the existence of OB associations.

Most of the ionized gas structures seem to expand from their place of birth into the ISM. As the relatively low escape velocity of the dwarfs will facilitate the removal of substantial amounts of interstellar matter, the question comes up whether these gaseous features stay gravitationally bound to the galactic disk (outflow) or whether they can escape from the gravitational potential by becoming a freely flowing wind (galactic wind). This is of special importance for the chemical evolution of galaxies, the enrichment of the intergalactic medium (IGM), and for the understanding of the formation of galaxies in the early universe (e.g., Recchi et al. 2004). The relative velocities of the ionized structures within about 1 kpc around the star forming regions are quite low (e.g., Martin 1998). Therefore, the gas appears to stay gravitationally bound to the host galaxies. No convincing case for a galactic wind has been found in a dwarf galaxy up to now (Bomans 2005). Nevertheless, galactic winds are generally regarded as a necessary ingredient to chemical and chemodynamical models of dwarf galaxies (e.g., Hensler et al. 2004). This apparent contradiction is most probably due to the previous inability to detect the faintest filaments at large distances from the host galaxies. The fastest moving shells most likely have the lowest densities, which corresponds to very low surface brightness in Hα.

We examined ionized gas structures around two dwarf galaxies which are very similar in mass, luminosity and shape. Very deep Hα images show previously undocumented ionized structures, some of them with sizes of several kpcs, located in the halos (e.g., van Eymeren et al. 2005). Furthermore, we performed high-resolution long-slit echelle spectroscopy covering several of the identified filaments in order to measure their gas kinematics. The most relevant parameters of the galaxies are listed in Table 1.

The distance of NGC 2366 and its position on the sky place this galaxy into the M 81 group. Nevertheless, it can be regarded as an isolated galaxy. Its appearance in Hα is dominated by the GEHR NGC 2363 in the south-western end of the galaxy.

Table 1. The sample of galaxies.

Parameters [unit]	NGC 2366	NGC 4861	References
Hubble type[a]	IB(s)m	SB(s)m	
m_B [mag]	−16.63	−16.62	(1)
D [Mpc]	3.44	7.5	(2), (3)
$v^a_{\rm sys}$ [km s^{-1}]	80	833	
$v_{\rm rot,\,H\,I}$ [km s^{-1}]	67	54	(4)
$\langle\sigma\rangle_{\rm H\,I}$ [km s^{-1}]	7.7	8.4	(4)
$\sigma_{\rm Peak,\,H\,I}$ [km s^{-1}]	14.3	19	(4)
i [°]	59	82	(4)
$M_{\rm H\,I}\left[10^9\,M_\odot\right]$	0.57	1.14	(4)

[a] Data from NED.
References: (1) Bomans (2001); (2) Tolstoy et al. (1995); (3) de Vaucouleurs et al. (1991); (4) Thuan et al. (2004).

This GEHR harbors two large OB associations, one in the core with an age of 1 Myr and one in the eastern part of the core with an age of 3−5 Myr (Drissen et al. 2001). NGC 4861 is very similar to NGC 2366 concerning its shape. It is also dominated by a GEHR in the south-west, I Zw 49, where most of the star formation occurs. A chain of small H II regions extends to the north-east. Although the galaxy shows almost no evidence for the existence of spiral structures (Wilcots et al. 1996), it is classified as SB(s)m. Its distance is more than twice the distance of NGC 2366 (see Table 1). Figure 1 shows our R band images of both galaxies.

This paper is organized as follows. The observations and the data reduction are described in Sect. 2. Section 3 presents the results of the imaging data. The catalog of the Hα filaments and shells can be found in Appendix A. In Sect. 4, the analysis of the echelle spectra including the detection of expanding material follows. A discussion of the results is presented in Sect. 5. Section 6 summerizes the main results.

2. Observation and data reduction

2.1. Optical imaging

Hα narrowband CCD images of the two irregular dwarf galaxies were required to establish a catalog of the Hα structures and to relate the slit positions of the spectra to the galaxies. Therefore, we used our image from the 3.5 m telescope of the Calar Alto Observatory (NGC 2366)[1] and archival data from the 3.6 m Canada France Hawaii Telescope (NGC 4861)[2], and from the HST (NGC 2363). After the standard data reduction with the software package IRAF, the corresponding continuum images were subtracted to produce images of the Hα line emission. In the case of the HST image of NGC 2363, no continuum-subtraction was done because no red continuum image was available. The image was flux-calibrated by using the photflam value for the Hα filter[3]. To estimate the contribution of the continuum and to define an error for the energy calculation in Sect. 5.1.1, we took a different continuum filter *F547M*, that was observed together with the *F656N*, scaled the flux of the stars to

[1] Based on observations collected at the Centro Astronómico Hispano Alemán (CAHA) at Calar Alto.

[2] Guest User, Canadian Astronomy Data Center, which is operated by the Dominion Astrophysical Observatory for the National Research Council of Canada's Herzberg Institute of Astrophysics.

[3] WFPC2 Data Handbook chapter 5, URL: `http://www.stsci.edu/instruments/wfpc2`

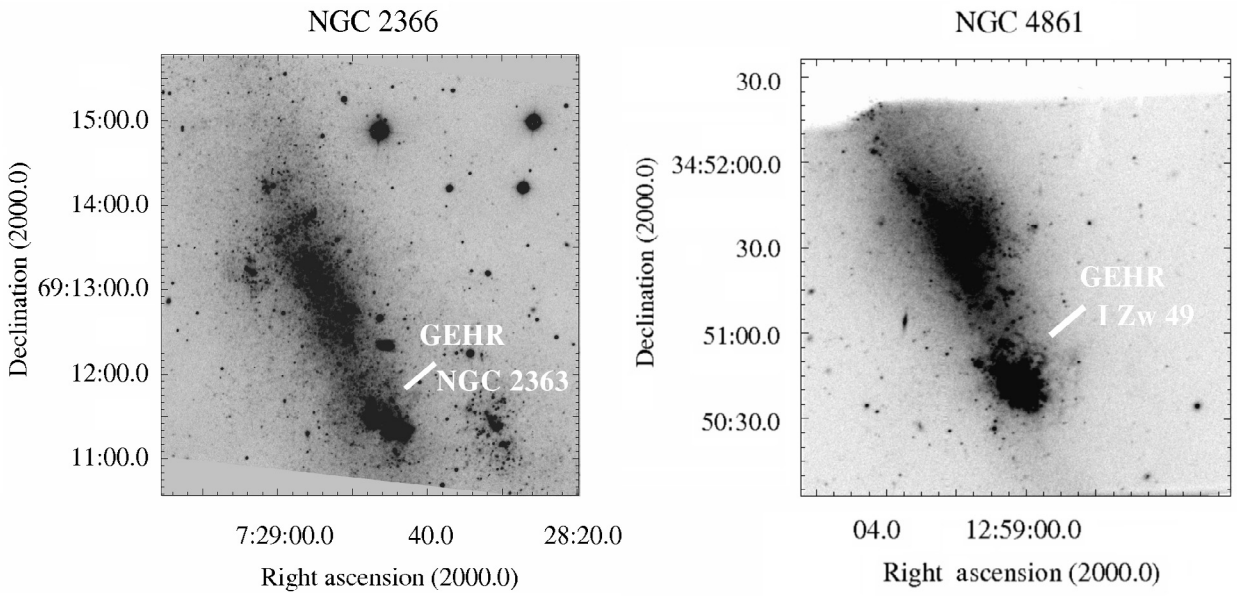

Fig. 1. *R* band images of NGC 2366 (*on the left*) and NGC 4861 (*on the right*). The GEHRs are marked in white. The white shadow on the top of NGC 4861 was caused by the pick up arm of the guider tracking a bright star in the northern part of the galaxy and also affects the Hα image (see Fig. 3). Therefore, the northern-most part of the galaxy is missing. Nevertheless, it is the deepest *R* band exposure of NGC 4861 available so far.

Table 2. Imaging – some observational parameters.

Parameters [unit]	NGC 2366	NGC 2363	NGC 4861
Date	14.01.91	08.01.96	12.03.00
Telescope/Instrument	3.5 m Calar Alto Prime Focus	HST WFPC2	3.6 m CFHT OSIS
Filter	658/10, Johnson R	F656N	6570/48, 6493/1305
Exposure time [s]	1200, 200	1500	900, 300
Scale [arcsec/pix]	0.38	0.1	0.15
FWHM [arcsec]	1.1	0.2	0.8

the stars in the Hα image and subtracted it from Hα. A comparison of the flux of the faint Hα filaments before the continuum-subtraction and afterwards shows that the flux is roughly 6% lower after the subtraction. As we expect that a continuum subtraction with a red filter is much more efficient than the one we did with *F547M*, the 6% give us an upper limit for the error. In Sect. 5.1.1, we calculate the energy by taking into account this uncertainty.

Finally, we used an adaptive filter which is based on the H-transform (Richter et al. 1991) to emphasize the weakest ionized gas features and to differentiate them from the noise.

Table 2 gives a short overview about the images.

2.2. Echelle spectroscopy of the Hα line

High-resolution long-slit echelle spectroscopy of both galaxies was performed with the 4 m telescope of the Kitt Peak National Observatory from March 18th to 20th 1998. Inserting a post-slit Hα filter with a width of 75 Å and replacing the cross dispersion grating by a flat mirror, we selected the Hα line at 6563 Å and the two [NII] lines at 6548 Å and 6583 Å. We picked the 79 lines mm^{-1} echelle grating with a blaze angle of 63°. The slit-width is about 240 μm (corresponding to 1.″6), which leads to an instrumental *FWHM* at the Hα line of about 13 km s^{-1}.

All data were recorded with the long focus red camera and a 2048 × 2048 Tek2 CCD. The pixel size is 0.08 Å along the dispersion and 0.″26 along the spatial axis. The slit-length was limited to 4′46″. The seeing was about 1″. For geometric distortion corrections we used star spectra, for the wavelength calibration we used spectra of a thorium-argon comparison lamp.

Close to the Hα emission of both galaxies, we additionally detected four night sky lines. In the spectra of NGC 4861 they could be subtracted by using the IRAF task *background*. For this correction Hα line-free parts along the spatial axis are needed. In the spectra of NGC 2366 the Hα emission is too extended to define an Hα line-free area and therefore to remove the night sky lines properly. However, due to the different redshifts of both galaxies, only the Hα emission of NGC 4861 is affected by one of these night sky lines. In the case of NGC 2366 the Hα emission lies clearly separated between two night sky lines so that this correction can be neglected.

The right panels of Figs. 2 and 3 show the slit positions of the spectra on the underlying continuum-subtracted Hα image. We obtained five spectra of each galaxy with small offsets from each other and with an exposure time of 1800 s (NGC 4861 all slits, NGC 2366 slit *01* and *02*) or 2400 s (NGC 2366 slit *03*, *04*, and *05*). The position angles were 40° for NGC 2366 and 0° for NGC 4861.

For the measurement of the emission lines the spectra were binned in the spatial direction by four pixels, which corresponds to about 1″ matching the seeing. At positions of very weak emission, we summed up over ten pixels and used the IRAF task *splot* in the interactive mode to determine the peak wavelength and the Full Width at Half Maximum (*FWHM*). At many locations, the emission line profile was double- or triple-peaked with clear minima in the intensity between these peaks. We fitted such

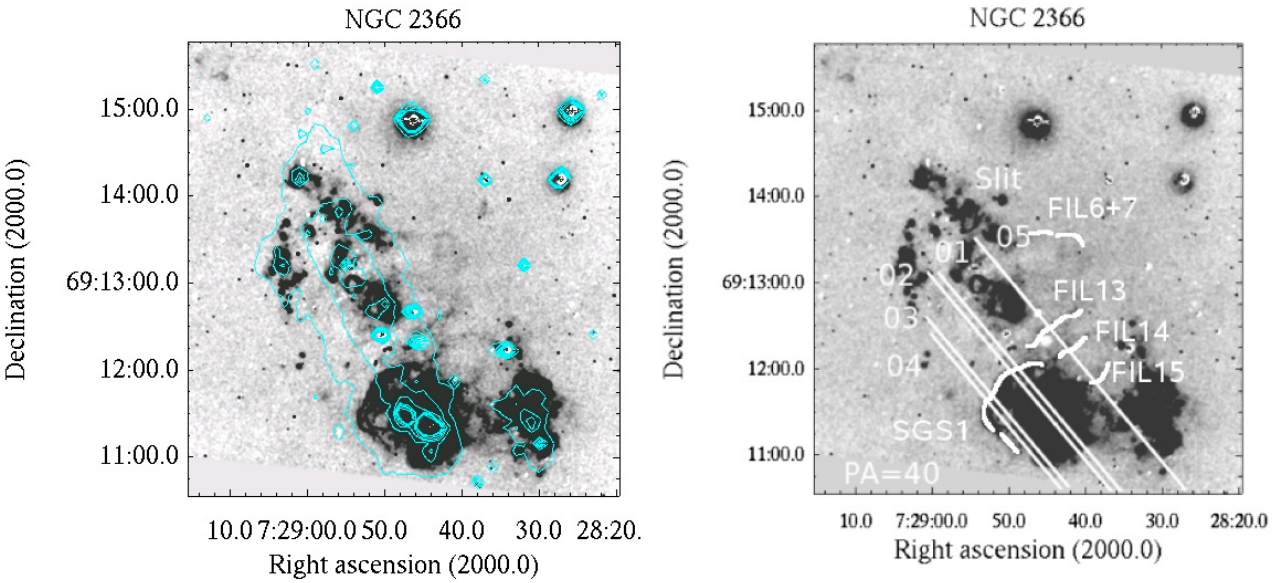

Fig. 2. NGC 2366. *Left panel*: continuum-subtracted Hα image with the continuum contours overlaid in blue (grey). *Right panel*: continuum-subtracted Hα image with the five slit positions indicated by white lines and the most important ionized gas structures also indicated by white lines. The upper end of each line representing a slit position indicates the end of the true slit. The true lower end of these slits as well as upper and lower end of the slits in NGC 4861 (see Fig. 3) are located outside of the Hα images.

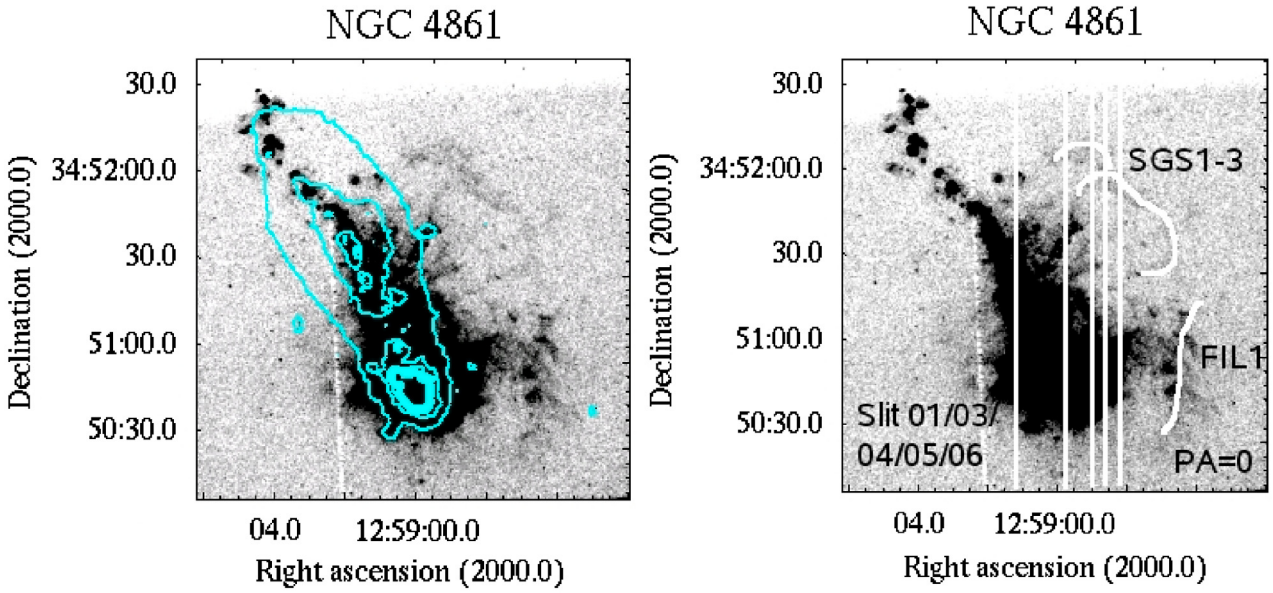

Fig. 3. NGC 4861. *Left panel*: continuum-subtracted Hα image with the continuum contours overlaid in blue (grey). *Right panel*: continuum-subtracted Hα image with the five slit positions indicated by white lines (the numbers are rising from *01* on the left to *06* on the right side of the image) and with the largest structures marked in white. The quality of slit *02* is too poor to give any reasonable results so that its position is left out on the right panel. The white shadow on the top was again caused by the pick up arm of the guiding camera (see Fig. 1) and hides the northern part of the galaxy.

profiles with two or three Gaussian components. The measured peak wavelengths were then converted into heliocentric velocities.

2.3. H I data

For a comparison of the measured Hα velocities with rotation curves derived from H I data, we used published H I moment maps by Thuan et al. (2004, their Figs. 1 and 7, bottom left panel). They used archival VLA data with a spatial resolution of 12.″5 (NGC 2366) and 15.″2 (NGC 4861). We copied the velocity information for the corresponding slit positions, which gives us a rough estimate for the behaviour of the neutral gas in comparison to the ionized gas.

3. Results – the catalog of filaments

Both galaxies show remarkable Hα features partly of kpc-size. We divided them into small scale (about a few hundred pc) and large scale structures (about 1 kpc and larger).

In the following subsections the structures of each galaxy are discussed. A complete catalog of the Hα structures can be found in Appendix A. All features were detectect by visual inspection

on our fully-reduced Hα images (see Figs. A.1 and A.2) and afterwards measured manually. Only structures above a 3σ detection limit were considered for this analysis. To measure the diameter of the superbubbles and supergiant shells, we began with the intensity maximum on one side of the ring and ended on the intensity maximum on the other side of the ring. The lengths of the filaments were measured by starting from one end at an intensity larger than 3σ and stopping at the other end before the intensity drops below 3σ. The errors for both measurements are about 0.″5 for each galaxy, which leads to 8 pc in the case of NGC 2366 and and 17 pc in the case of NGC 4861. The lower detection limit depends on the resolution and is 17 pc in the case of NGC 2366 (*FWHM* of 1.″1, see Table 2) and 27 pc in the case of NGC 4861 (*FWHM* of 0.″8).

3.1. NGC 2366

3.1.1. Small scale structures

NGC 2366 shows a wealth of small structures especially around the GEHR NGC 2363 and in the north-eastern part of its tail (Fig. A.1). These filaments have sizes of about a few hundred pc (see Table A.1). Most of them surround NGC 2363 and seem to connect the GEHR to the small H II region in the west. All filaments in the eastern part of NGC 2363 are located at the inner edge of the supergiant shell SGS1. Another important structure is the diffuse ionized gas in the north-western part of NGC 2363. It is represented by a few small filaments (e.g., FIL14 and FIL15) which are all perpendicular to the major axis of NGC 2366. FIL14 and FIL15 form the edges of an enormous outflow, which is discussed in Sect. 4.1.1.

Altogether it seems that many of the smaller filaments connect the GEHR to the large scale structures (e.g., SGS1) or to other H II regions.

3.1.2. Large scale structures

The largest structure in NGC 2366 is the above mentioned supergiant shell SGS1 which was detected before by Bomans & Hopp (1992) – their shell 1 –, Hunter et al. (1993) – their features 1 and 2 –, and Martin (1998) – her feature A –. It is located at the north-eastern part of the GEHR at a distance of about 850 pc from the center of NGC 2363 and has a diameter of about 900 pc. It is connected to the GEHR via the smaller filaments as discussed above. FIL6 and FIL7 together with FIL13 in the northern part of the galaxy may form the edge of a giant shell which has fragmented as described in Sect. 1. It then would have had a diameter of about 1 kpc.

3.2. NGC 4861

3.2.1. Small scale structures

Comparable to NGC 2366, NGC 4861 shows a high amount of smaller structures around its GEHR I Zw 49 (Fig. A.2, Table A.2). But in this case, a lack of ionized filaments exists in the north-eastern part of the GEHR. In the western part, a complex web of filaments is visible on the Hα image, which we detected as expanding material in our spectra. Especially FIL9 to FIL11 at the western part of the tail, which extend perpendicular to the major axis of NGC 4861, seem to form a connection to the large scale structure mentioned below.

The upper part of the tail of NGC 4861 mainly consists of small H II regions and shows no diffuse filamentary emission. The white shadow on the top of the image was caused by the pick up arm of the guiding camera tracking a bright star in the northern part of the galaxy. This does not affect the analysis because, as mentioned above, no ionized gas structures were found around this area.

3.2.2. Large scale structures

The most prominent features in NGC 4861 are the kpc-sized filaments extending from the north to the west of I Zw 49 (SGS1-3, FIL1, see Fig. 3 right panel). Assuming that SGS1, SGS2 and SGS3 belong to one single shell, it would have a diameter larger than 2 kpc.

4. Results – the kinematics of the ionized gas

Figure B.1 presents the echellograms grouped by galaxy and arranged in a spatial sequence. A first glance reveals a large amount of velocity structures. In a first step, we looked for expanding gas and tried to connect the emission features to the cataloged structures. Partially, a Doppler ellipse as described in Martin (1998) was detected, which gives evidence for an expanding shell structure. In some cases, we only detected emission at a constant wavelength which is Doppler-shifted with respect to the rest wavelength of the galaxy (measured in H I). This indicates an expanding outflow. The following sections present the results of our search.

4.1. Detections of expanding material in the individual galaxies

4.1.1. NGC 2366

Figure 4 shows the position–velocity (pv) diagram of the Hα emission in NGC 2366, Fig. 5 shows an enlargement of the core region in slits *01* and *02*. The solid line marks the velocities of the H I gas which are derived from the H I maps of Thuan et al. (2004) and which represent the circular velocity of the galaxy (corrected for the redshift of the galaxy). The cross marks define the heliocentric Hα velocities corrected for the redshift of the galaxy, which indicates the radial expansion velocities of the ionized gas compared to the H I velocities. The location of the continuum emission in slit *01* indicating stars and therefore the center of the GEHR is set to 0″.

Generally, the velocity of the Hα emission agrees with the velocity of the neutral hydrogen, which means that it takes part in the rotational motion of the galaxy. But at some positions there are significant deviations from the H I velocities. Spectrum *05* shows a blue-shifted component with a length of about 700 pc and an expansion velocity of about 30 km s^{-1} (marked as OF in Fig. 4). As mentioned above, this outflow is directly correlated with some of our detected filaments on the Hα image (especially with FIL14 and FIL15). Probably, there is a connection between the outflow and some detections of the Hα emission leaving the GEHR NGC 2363 to the north-west (Roy et al. 1991; Martin 1998), which means that the ionized gas cone is larger than assumed before (see Fig. 6).

The supergiant shell SGS1 (see Sect. 3) is also detected in the pv diagram. Unfortunately, the emission of the GEHR is so bright that it outshines all weaker emission features. Still, one can notice a small gap between the edge of the shell and the bright core of NGC 2363 (see Fig. 2). In this region the Hα emission splits into two components, one blue-shifted and one red-shifted compared to the H I velocity. From these

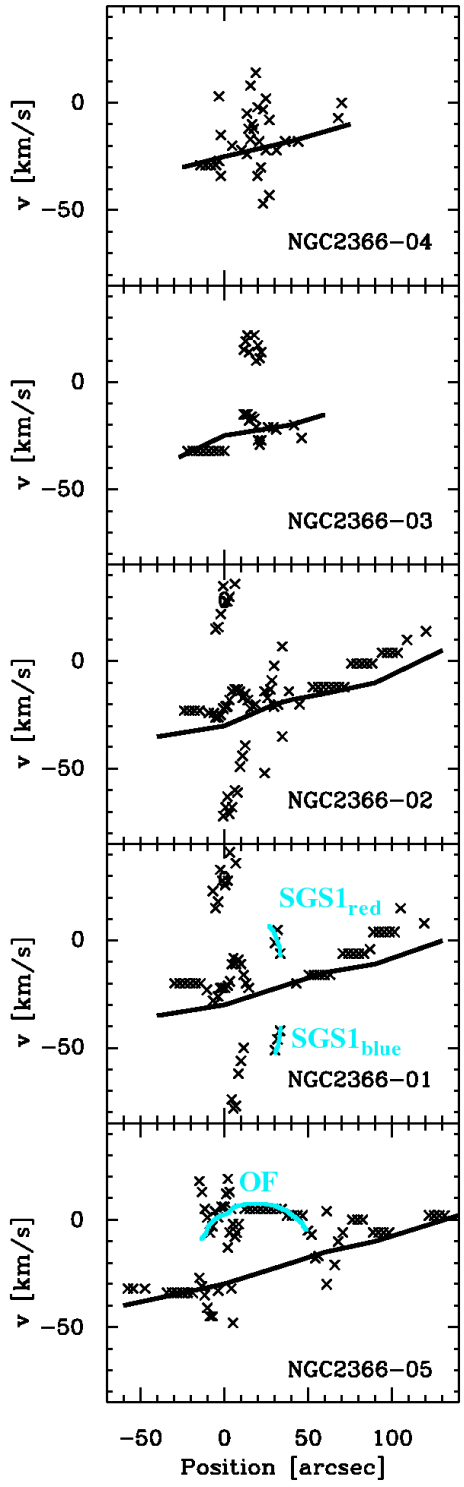

Fig. 4. NGC 2366: position–velocity diagrams of all slits arranged in a spatial sequence. The crosses mark the Hα velocities, the solid line represents the rotational motion of the galaxy derived from H I maps by Thuan et al. (2004). The most prominent ionized gas structures are marked in blue (grey). Referring to the position: positive values go to the north-east. The measurement of the Hα peak velocity is very accurate and errors are only about few km s^{-1}, here indicated by the size of the crosses. The errors of the H I velocity are smaller than 5 km s^{-1}.

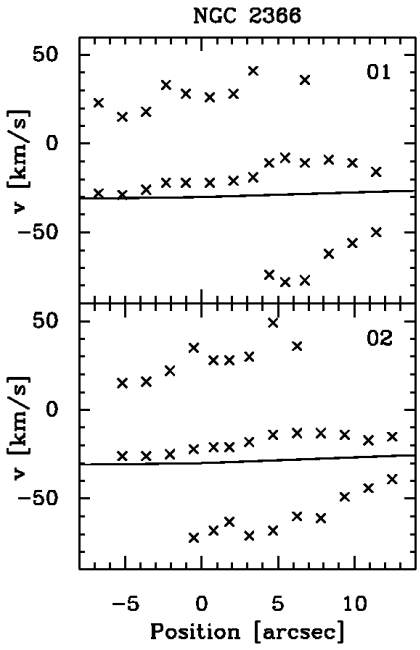

Fig. 5. Enlargement of the core region in slit *01* and slit *02*.

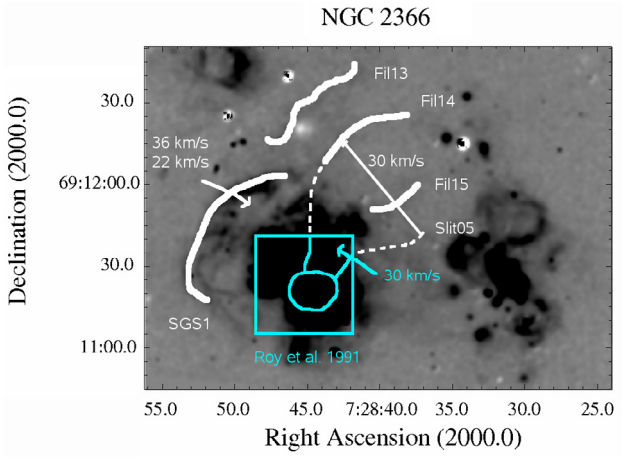

Fig. 6. Scheme of the north-western outflow of NGC 2366. In blue (grey) the results of Roy et al. (1991), in white our results. Slit 05: only the velocity offset of 30 km s^{-1} is marked.

measured velocities we estimate the expansion velocity of the shell, assuming that the shell forms a hemisphere with a radius of 470 pc and expands unequally. The unequal expansion can be seen on the pv diagram of spectrum *01* at 30″ (SGS1$_{\rm red}$ and SGS1$_{\rm blue}$). The red-shifted component shows lower velocities compared to the H I data than the blue-shifted component. We derive as an upper limit 36 km s^{-1} blue-shifted and 22 km s^{-1} red-shifted, which are very moderate expansion velocities.

Apart from these striking features we generally see a lot of turbulence in the core region of NGC 2366. This is shown in all slits around position 0″ (Fig. 4). The Hα emission splits into three components, one following the H I velocity, one blue-shifted and one red-shifted. The enlargement of the core region of slit *01* and slit *02* (see Fig. 5) clearly shows the three separate components.

4.1.2. NGC 4861

NGC 4861 shows a complex field of ionized gas structures which is very similar to NGC 2366 (see Sect. 3). Due to the limited throughput of the echelle spectrograph and unstable weather

conditions during some parts of the observation, we only detect the emission of the luminous GEHR I Zw 49. The faint and very interesting structures in the north-west of the galaxy (SGS1, SGS2, SGS3) are not visible in our spectra. Nevertheless, we find some striking features in the pv diagrams (Fig. 7). In this case, the location of the continuum emission in slit *03* was set to 0″. Slit *02* was left out as the quality of the spectrum was too poor to give any reasonable results.

In all spectra but spectrum *01*, the Hα emission splits into several components. One component follows the rotational motion of the galaxy (H I data by Thuan et al. 2004). Additionally, we find in all spectra but *01* a blue-shifted component which partly has the appearance of a Doppler ellipse (SGS4$_{\rm blue}$). The radial expansion velocity declines from 110 km s^{-1} (spectrum *03*) to 60 km s^{-1} (spectrum *06*). In spectra *03* and *04*, there is also a red-shifted component with an expansion velocity of 40 km s^{-1} and 30 km s^{-1} respectively (SGS4$_{\rm red}$). The blue-shifted component may be a part of an expanding shell with an expansion velocity of at least 110 km s^{-1}. The expanding material corresponds to the web of gaseous filaments in the western part of I Zw 49 (Fig. A.2). It is limited by FIL1 which could represent the outer edge of the expanding shell. The red-shifted component could belong to the same shell, but to verify this presumption, we need deeper spectra of the whole galaxy. As the GEHR outshines all additional emission line components, this shell cannot be detected on the Hα image. Still, it is added with a blue- and a red-shifted part to the list of ionized gas structures in Table A.2 as SGS4. Its diameter was estimated from slit *03*.

The western outflow mentioned above was also found by Martin (1998). She even detected a bipolar outflow going to the east and west of the galaxy. We cannot verify the eastern outflow as we have no slit located at this position. Instead, we also detect some outflowing gas in the northern part of the GEHR (see Fig. 7, slit *01* and slit *03* OF), which is described by Martin (1998) as a faint red wing.

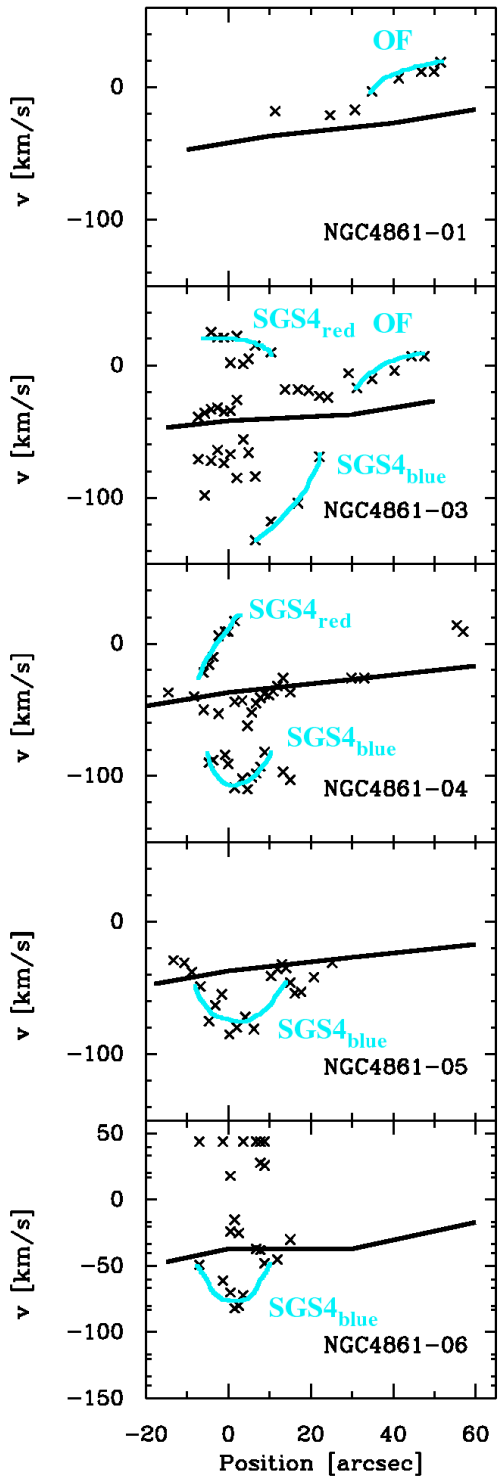

Fig. 7. NGC 4861: position–velocity diagrams of all slits arranged in a spatial sequence. The crosses mark the Hα velocities, the solid line represents the rotational motion of the galaxy derived from H I maps by Thuan et al. (2004). The most prominent ionized gas structures are marked in blue (grey). Referring to the position: positive values go to the north. The measurement of the Hα peak velocity is very accurate and errors are only about few km s^{-1}, here indicated by the size of the crosses. The errors of the H I velocity are smaller than 5 km s^{-1}.

5. Discussion

5.1. A complex web of filaments and their kinematics

We found ionized shells and filaments in both galaxies, whereby the amount of shell-like structures in comparison to the amount of filaments is very small, although some of the filaments could be the relicts of former shell structures.

We divided all ionized gas features into small and large scale structures. Many small scale structures are larger than 300 pc, and we detected several large scale structures up to a size of 2 kpc. In many cases it seems that in both galaxies the smaller filaments connect the prominent H II region to the large scale structures or to smaller H II regions as in the case of NGC 2366. Both galaxies contain some kpc-sized filaments which are parallel to their major axes (e.g., SGS1-3 in NGC 4861). H I intensity maps (Thuan et al. 2004) show that the neutral gas is much more extended than the ionized gas. That implies that the ionized shells are running into an extended H I envelope, which leads to some interaction between both phases. Unfortunately, our echelle spectra do not give any kinematic information about those shells so that we cannot make any statements on which processes happen in the halo. Deeper spectra and Fabry-Pérot interferometry are proposed to improve the sensitivity of our observations.

Kpc-scale expanding shells which are elongated in the general direction of the H I minor axis were found before in amorphous dwarfs (Marlowe et al. 1995) and in I Zw 18 (Martin 1996). Furthermore, narrow elongated filaments which seem to connect the disk with the halo were recently detected in spiral galaxies by Rossa et al. (2004).

Especially NGC 4861 shows these huge supergiant shells (SGS1-3) and several finger-like structures (FIL9-11) which emanate from the disk into the halo and seem to connect the disk with the shells. The chimney scenario (see Sect. 1) is one possible explanation. Another explanation are Rayleigh-Taylor instabilities. If two neighboring gas layers of different density are perturbed, potential energy is released in the sense that the heavier material moves down under the gravitational field and the lighter material is displaced upwards. That means in our case that under the assumption that SGS1-3 have once formed a single shell, this shell has ruptured at some points and the gas is now falling down. This downfalling gas has the appearance of a finger, which is exactly what we see on the Hα image.

Referring to these large scale structures, we have to check their expansion velocities by obtaining deeper spectra than the currently available echelle spectra. Only then we can make precise statements on their evolution. The spectra of NGC 2366 already indicate that the gas near the perpendicular filaments expands from the GEHR, whereas we have no such information on NGC 4861.

Most of the smaller and disk-near expanding ionized gas structures which we found in the echelle spectra can be correlated to the identified features in the Hα images. Some of the features have the appearance of a Doppler ellipse in the pv diagram or they form at least a part of a Doppler ellipse as can be seen in e.g., Figs. B.1 and 7, slit *05* of NGC 4861. At many other positions, we just detect a constant, Doppler-shifted component (e.g., Fig. 4 slit *03*).

The expansion velocities are usually very moderate (up to 50 km s^{-1}), but in NGC 4861, we found an expanding shell with a velocity of about 110 km s^{-1}.

5.1.1. The origin of the expanding shells

We want to study one of our detected shells in more detail: SGS1 in NGC 2366 is found to expand unequally with very moderate velocities (see Sect. 4.1.1). One reason for an unequally expanding shell are possible density inhomogeneities. Probably, the gas density behind the shell is higher than in front of it (along our line of sight). Thus, the ionized gas shell has to push more material if the density is higher, which leads to a deceleration of its expansion velocity. We also estimated the kinetic energy of this shell under the assumption of a very thin hemisphere of radius $r = 470$ pc and thickness $\delta r = 5$ pc. The mass was calculated from the flux-calibrated HST image (see Sect. 2.1). We get a kinetic energy of $E(\mathrm{H}^+) = 4.6 \times 10^{50}$ erg. This is just an upper limit as we overestimate the Hα flux (see Sect. 2.1). Taking into account the error of the flux calibration, we get a value that is 3% lower.

The age of expansion can be estimated (under the assumption of a constant expansion) from $t \approx \frac{R}{v_{\mathrm{exp}}}$, which gives us about 10^7 years. Comparing this to the ages of the two local star clusters (1 and 5 Myr old respectively) results in the conclusion that we do need a former star formation event. Nevertheless, there must be another excitation or ionization mechanism which keeps the shell expanding. This could possibly be done by stellar winds from the two current star clusters.

5.1.2. Large line widths in NGC 2366 and NGC 4861

The shells and filaments and especially the GEHRs of both galaxies show a Full Width at Half Maximum (*FWHM*) of about 30 to 50 km s^{-1} (corrected for instrumental broadening). This gives us a velocity dispersion of 11 to 19 km s^{-1}. These values are comparable to those of GEHRs (Hunter & Gallagher 1997). But GEHRs harbor large OB associations as energy source, whereas no such energy sources exist around most of the detected filaments. Hunter & Gallagher (1997) explain such a high dispersion with a high dispersion of the H I gas. Looking at the velocity dispersion of the neutral hydrogen (see Table 1), the Hα dispersion is higher than the average H I dispersion, but fits well the peak dispersion (NGC 2366: 14.3 km s^{-1}, NGC 4861: 19 km s^{-1}). A comparison with the H I peak dispersion is more reliable as we trace Hα only in the central regions of the galaxies. Therefore, our observations prove the statement of Hunter & Gallagher (1997).

The question is now why especially the GEHRs of both galaxies show such a high *FWHM* (e.g., the GEHR of NGC 2366 splits into three different components). A work by Yang et al. (1996) examined the most luminous H II region NGC 604 in M 33. They also found broadened Hα lines with *FWHM*s of about 40 km s^{-1}. If one assumes the thermal component of Hα to be 20 km s^{-1}, these high *FWHM*s cannot only be explained by thermal broadening. Other mechanisms which are suggested and discussed by Yang et al. (1996) are stellar winds, and supernova remnants.

5.2. Outflow or galactic wind?

Our results of both Hα imaging and echelle spectroscopy lead to the question of the fate of the expanding gas. To determine whether it can escape from the gravitational potential (galactic wind) or not (outflow), we compared its expansion velocity to the escape velocity calculated by using the dark matter halo model by Navarro et al. (1996), for short NFW-model. In this model, the galaxy is dominated by a halo of dark matter, and the baryonic matter of the disk is neglected. The circular and the escape velocity were calculated by

$$v_{\mathrm{rot}} = \sqrt{\frac{G\,M_{\mathrm{s}}}{3}\,\frac{r}{(r+r_{\mathrm{s}})^2}} \tag{1}$$

and

$$v_{\mathrm{esc}} = \sqrt{2\left|-\frac{G\,M_{\mathrm{s}}}{r}\log\left(1+\frac{r}{r_{\mathrm{s}}}\right)\right|}. \tag{2}$$

We compiled the pv diagrams of NGC 2366 and NGC 4861, where position 0 corresponds to the dynamic center of the galaxies and all velocities are corrected for the redshift.

In the case of both galaxies, we used the H I data by Thuan et al. (2004). By varying the reference mass M_{s} and the virial radius r_{s}, we calculated the rotation curves (using Eq. (1)) in order to get the best approximation to the H I data. In Figs. 8 and 9, two different parameter sets (M_{s} and r_{s}) for each galaxy are shown. Using the same reference masses and virial radii than for the rotation curves, we calculated the escape velocities by Eq. (2). Additionally, we plotted the expansion velocities of our detected outflows at the corresponding distance from the dynamic center of the galaxies.

Tables A.1 and A.2 show several filaments and shells that could also be detected on the slit spectra. In most of the cases, one prominent structure is based on several smaller structures, e.g., in NGC 2366 all filaments from FIL24 to FIL28 belong to the supergiant shell SGS1. Therefore, we only consider the most prominent structures for our analysis, i.e. the hemisphere limited by SGS1 (the radial velocities have been estimated in Sect. 4.1.1)

and the north-western outflow marked by FIL14 and FIL15 in NGC 2366 and the supergiant shell visible on the pv diagrams in NGC 4861 (see Sect. 4.1.2). All other structures are not well-defined so that we cannot tell anything about their symmetry and therefore about their true expansion velocity.

As we assume a spherical symmetry for both expanding shells around the GEHRs of NGC 2366 and NGC 4861, the expansion velocities do not need to be corrected for the inclination of the galaxies. At every position where we intersect the shells we get the true expansion velocity. In the case of the outflow in NGC 2366, we cannot define a geometry. But if one assumes an inclination angle of 59°, measured from H I observations (see Table 1), we get an expansion velocity of 35 km s^{-1} instead of our measured value of 30 km s^{-1}, which gives a velocity increase of only 17%, still far below the derived escape velocity of the galaxy.

The chosen size of the reference mass is in all cases by orders one or two higher than the H I mass derived from the H I velocity maps (see Table 1). That means that the determination of the mass of the galaxy from the H I velocities is only a rough estimate.

A comparison of the H I data with the rotation curves derived from Eq. (1) shows that neglecting the cores of dwarf galaxies leads to a discrepancy between the dark matter halo rotation curves and the observed H I data at small distances from the dynamic center. That means that the baryonic matter in the disk has a significant influence on the rotation of the galaxy near the dynamic center. In the outer parts, dwarf galaxies are dominated by the dark matter halo.

5.2.1. NGC 2366

NGC 2366 is dominated by the GEHR NGC 2363. Several ionized structures emanate from this actively star-forming region. Both the expansion velocities of the shell SGS1 and the outflow to the north-west of NGC 2363 are shown in Fig. 8. Plotted are the beginning and the end point of the structures corresponding to their distances from the dynamic center. SGS1 is presented with both expansion velocities. As we had to choose very high reference masses in comparison to the H I mass of the galaxies to fit the rotation curve to the H I data, we get very high escape velocities of about 200 km s^{-1} and higher. The expansion velocities are moderate and remain far below the escape velocities. That means that the gas is still gravitationally bound to the galaxy.

One has to have in mind that at least the velocity of the western outflow is just a radial velocity. The real velocity will be higher so that our values just represent a lower limit of the expansion velocities.

5.2.2. NGC 4861

In NGC 4861 (Fig. 9) we have a similar situation as in NGC 2366. We found one large outflow which probably forms an expanding shell. The value of the red-shifted component is moderate (<40 km s^{-1}) and remains far below the escape velocity of the galaxy. The blue-shifted component of the outflow expands with a much higher velocity (about 110 km s^{-1}) and therefore nearly reaches the escape velocity, at least in the case of the lower values for mass and virial radius. But when looking at the corresponding rotation curve it becomes obvious that choosing a low mass and a low virial radius gives us a very poor model to the H I velocities of Thuan et al. (2004). From a distance r of 2.5 kpc on, which corresponds to the position of the outflow,

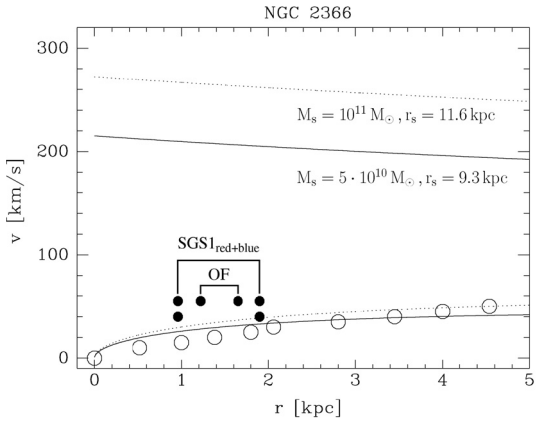

Fig. 8. Position–velocity diagram of NGC 2366. Different velocities are plotted versus the distance from the dynamic center of the galaxy. The solid and dashed lines represent two different parameter sets of the mass and the radius. The rotation curves follow more or less the H I position–velocity data described in Thuan et al. (2004), here drawn as open symbols. The lines in the upper part show the escape velocity. The expansion velocities of our detected shells and outflows are presented as solid symbols (beginning and end point of each structure). Referring to the velocity, the sizes of the solid and open symbols show the errors which are about 5 km s^{-1} for measuring the expansion velocity and about 10 km s^{-1} for the H I velocities. Positional errors are negligible. Therefore, they are not presented here.

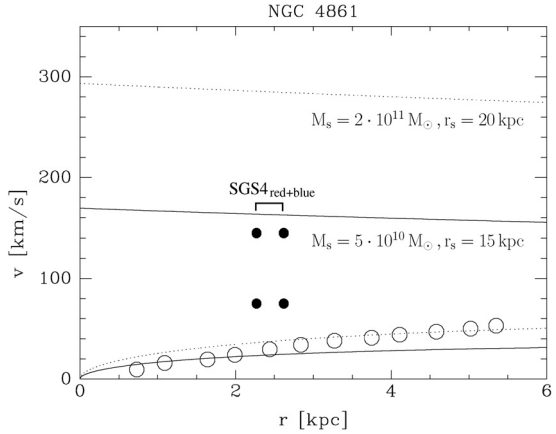

Fig. 9. Position–velocity diagram of NGC 4861. The same as in Fig. 8. The H I data are again taken from Thuan et al. (2004).

the H I rotation curve and the model are not in good agreement. Only by going to higher masses and higher virial radii, this fit can be improved, which implies that the escape velocity is rising and that therefore the faster expanding part of the shell definitely stays below the escape velocity.

5.3. Outflow!

Both galaxies show outflows with expansion velocities between 20 and 110 km s^{-1}. Generally, these velocities stay below the escape velocities of the galaxies derived from the NFW-model.

A comparison of our results with the 1d chemodynamical models of Hensler et al. (2004) shows that in the end the dark matter defines the fate of the expanding gas. Their models predict that most of the gas (galaxy mass of $\sim 10^9\,M_\odot$) or even all the gas (galaxy mass of $\sim 10^{10}\,M_\odot$) can leave the gravitational potential as a galactic wind by neglecting the dark matter. Therefore,

no further star formation due to a new collapse of the gas is possible. However, the presence of dark matter increases the escape velocity of the galaxy. The gas cannot flow out that easily so that the galaxy is enriched by metals and further star formation can take place. This could be true for our sample galaxies. In both of them we detected gas which seems to flow out of the galactic disk, but stays closely to the galaxy (see Sect. 3). We measured the expansion velocities of some of these structures, which are relatively moderate and not sufficient for a galactic wind. A comparison with the models of Mac Low & Ferrara (1999), see our Sect. 1, confirms our results.

Martin (1998) also used dark matter halo models to compare the escape velocity of the galaxies to the expansion velocities of the shells. She showed that only the smallest galaxies of her sample, Sextans A and I Zw 18, have shells with expansion velocities comparable to the escape velocities. Otherwise, the expansion velocities lie far below the escape velocities.

That means that we have to look at galaxies of very low mass when hunting for galactic wind structures. On the other hand, it is not clear yet what happens to the large scale structures at kpc distances from the galactic disk. Neither Martin (1998) nor we were able to detect them in the spectra.

Therefore, our next steps are further investigations of these two and other dwarf galaxies. We especially have to find a method to detect the weakest emission in the halos of the galaxies.

6. Summary

We examined two irregular dwarf galaxies which are very similar according to their mass, shape and luminosity.

First, we used Hα images to create a catalog of shells and filaments (see Appendix A). We performed high-resolution long-slit echelle spectroscopy of the most prominent emission features in order to analyze their kinematics. Finally, we used dark matter halo models to get an idea whether the expanding structures can leave the gravitational potential or not.

In both galaxies we found both small scale (up to a few hundred pc) and large scale (about 1−2 kpc) ionized gas structures. The GEHRs are mainly surrounded by smaller filaments which sometimes seem to connect the GEHRs to the large scale filaments or to neighboring H II regions (e.g., in NGC 2366). Especially in the outer parts of the galaxies, the filaments have large scale sizes. They are located at distances up to several kpc away from any place of current star formation. Thus, one has to think about the ionizing processes. Probably, the ionizing OB association has already died and the shells and filaments are only some relicts of a former star formation event. This would give us direct hints with respect to the age and the development of galaxies.

Furthermore, we need to explain the disrupted structure of the giant shells and the connecting filaments between the disk and the halo. As we do not have any kinematic information, we cannot prove whether these structures can be caused by Rayleigh-Taylor instabilities, finger-like emanating gas according to the chimney model or interaction with a surrounding H I envelope, just to mention a few possible scenarios. This has to be investigated in more detail with much deeper data.

Both galaxies show outflowing material. The expansion velocity varies from 20 km s^{-1} to 110 km s^{-1}. Using the dark matter halo model by Navarro et al. (1996) in order to compare the expansion velocities to the escape velocities of the galaxies, we found that in all cases the expansion velocity stays below the escape velocity. This result fits to the predictions of Mac Low & Ferrara (1999) and the studies of Martin (1998), but it does not fit to the 1d chemodynamical models of Hensler et al. (2004). It draws our attention to the faint large scale structures in the outer parts of the galaxies and to mass-poor galaxies with a low gravitational potential.

Acknowledgements. The authors would like to thank U. Hopp for providing his image of NGC 2366. We thank Lutz Haberzettl, Chaitra Narayan, and Clemens Trachternach for helpful comments and useful discussions.
This research made use of the NASA's Astrophysics Data System Abstract Service, the LEDA database (`http://leda.univ-lyon1.fr`), and the NASA/IPAC Extragalactic Database (NED) which is operated by the Jet Propulsion Laboratory, California Institute of Technology, under contract with NASA.

References

Birk, G. T., Lesch, H., & Neukirch, T. 1998, MNRAS, 296, 165
Bomans, D. J. 2001, Ap&SS, 276, 783
Bomans, D. J. 2005, in The Evolution of Starbursts, AIP Conf. Proc., 783, 98
Bomans, D. J., & Hopp, U. 1992, in Evolution of Interstellar Matter and Dynamics of Galaxies, ed. J. Palous, W. B. Burton, & P. O. Lindblad, 63
Bomans, D. J., Chu, Y., & Hopp, U. 1997, AJ, 113, 1678
de Vaucouleurs, G., de Vaucouleurs, A., Corwin, H. G., et al. 1991, Third Reference Catalogue of Bright Galaxies (Berlin, Heidelberg, New York: Springer-Verlag), 1
Drissen, L., Crowther, P. A., Smith, L. J., et al. 2001, ApJ, 546, 484
Gallagher, J. S., & Hunter, D. A. 1984, ARA&A, 22, 37
Hensler, G., Theis, C., & Gallagher, J. S., I. 2004, AAP, 426, 25
Hunter, D. A., & Gallagher, J. S. 1997, ApJ, 475, 65
Hunter, D. A., Hawley, W. N., & Gallagher, J. S. 1993, AJ, 106, 1797
Mac Low, M., & Ferrara, A. 1999, ApJ, 513, 142
Marlowe, A. T., Heckman, T. M., Wyse, R. F. G., & Schommer, R. 1995, ApJ, 438, 563
Martin, C. L. 1996, ApJ, 465, 680
Martin, C. L. 1998, ApJ, 506, 222
Navarro, J. F., Frenk, C. S., & White, S. D. M. 1996, ApJ, 462, 563
Norman, C. A., & Ikeuchi, S. 1989, ApJ, 345, 372
Recchi, S., Matteucci, F., D'Ercole, A., & Tosi, M. 2004, AAP, 426, 37
Richter, G. M., Lorenz, H., Bohm, P., & Priebe, A. 1991, Astron. Nachr., 312, 345
Rossa, J., Dettmar, R.-J., Walterbos, R. A. M., & Norman, C. A. 2004, AJ, 128, 674
Roy, J., Boulesteix, J., Joncas, G., & Grundseth, B. 1991, ApJ, 367, 141
Shapiro, P. R., & Field, G. B. 1976, ApJ, 205, 762
Silich, S., & Tenorio-Tagle, G. 2001, ApJ, 552, 91
Slavin, J. D., Shull, J. M., & Begelman, M. C. 1993, ApJ, 407, 83
Thuan, T. X., Hibbard, J. E., & Lévrier, F. 2004, AJ, 128, 617
Tolstoy, E., Saha, A., Hoessel, J. G., & McQuade, K. 1995, AJ, 110, 1640
van Eymeren, J., Bomans, D. J., & Weis, K. 2005, in The Evolution of Starbursts, AIP Conf. Proc., 783, 116
Wilcots, E. M., Lehman, C., & Miller, B. 1996, AJ, 111, 1575
Yang, H., Chu, Y.-H., Skillman, E. D., & Terlevich, R. 1996, AJ, 112, 146

Online Material

Table A.1. The most prominent structures and their sizes in NGC 2366.

Source	Diameter [″]	Diameter [pc]	$v_{\rm helio}$ [km s^{-1}]	*FWHM* [km s^{-1}]
SGS1	59	940	49/99	26/38
SB1	11	180		
SB2	19	300		
SB3	9	150		
Source	**Length [″]**	**Length [pc]**	$v_{\rm helio}$ [km s^{-1}]	*FWHM* [km s^{-1}]
FIL1	7	110		
FIL2	32	510		
FIL3	14	230		
FIL4	9	140		
FIL5	10	160		
FIL6	23	370		
FIL7	17	270		
FIL8	19	300		
FIL9	7	110		
FIL10	9	150		
FIL11	21	330		
FIL12	15	240		
FIL13	51	820	95	33
FIL14	19	300	107	29
FIL15	23	360	92	46
FIL16	11	180		
FIL17	18	280		
FIL18	21	330		
FIL19	37	590		
FIL20	6	100		
FIL21	10	160		
FIL22	17	270		
FIL23	12	190		
FIL24	11	180	81	37
FIL25	25	400	78	50
FIL26	13	200	84	40
FIL27	5	80	83	41
FIL28	6	100	79	33

Note: $v_{\rm exp}$ and the *FWHM* (corrected for instrumental broadening) are added when the ionized gas features were also detected in the spectra. The first part of the table contains the ring-like features which are divided into superbubbles (SB, with a diameter smaller than 500 pc) and supergiant shells (SGS, with a diameter larger than 500 pc). All other structures are presented in the second part of the table as filaments (FIL, all lengths). The same classification is also used for Table A.2.

Table A.2. The most prominent structures and their sizes in NGC 4861.

Source	Diameter [″]	Diameter [pc]	$v_{\rm helio}$ [km s^{-1}]	*FWHM* [km s^{-1}]
SGS1	22	800		
SGS2	20	730		
SGS3	24	890		
SGS4[a]	30	1091	699/842	22/55
SB1	8	300	836	40
SB2	4	140	814	38
Source	**Length [″]**	**Length [pc]**	$v_{\rm helio}$ [km s^{-1}]	*FWHM* [km s^{-1}]
FIL1	49	1770		
FIL2	5	170		
FIL3	29	1070		
FIL4	11	400	799	41
FIL5	18	640	823	31
FIL6	3	110		
FIL7	2	70		
FIL8	5	170		
FIL9	12	440		
FIL10	18	650		
FIL11	26	940	842	36
FIL12	6	200		
FIL13	4	130		
FIL14	5	190		
FIL15	13	470		
FIL16	7	270		
FIL17	7	240		
FIL18	4	140		
FIL19	5	180		
FIL20	5	180		
FIL21	5	170		
FIL22	15	530		
FIL23	17	620	793	40
FIL24	6	220		
FIL25	13	480	751	36
FIL26	9	330		
FIL27	3	100		
FIL28	2	70	797	28
FIL29	9	340	794	40
FIL30	6	200	797	36
FIL31	5	180		

[a] This shell was not detected on the Hα image of NGC 4861 because the GEHR outshines all additional emission. The diameter of SGS4 was therefore estimated from the Doppler ellipse in slit *03*.

Appendix A: The Hα images and catalogs

Here, we present the continuum-subtracted Hα images of NGC 2366 and NGC 4861 with the ionized gas structures marked in white. Additionally, the identified gas features are listed in the following tables. We measured the angular sizes of the ring-like structures and the filaments and converted them to linear sizes assuming the distances given in Table 1. For the detection method and the measurements of the structures see Sect. 3.

For all structures we could identify in our spectra the values of the heliocentric velocity and the *FWHM* (corrected for instrumental broadening) are also presented in Tables A.1 and A.2.

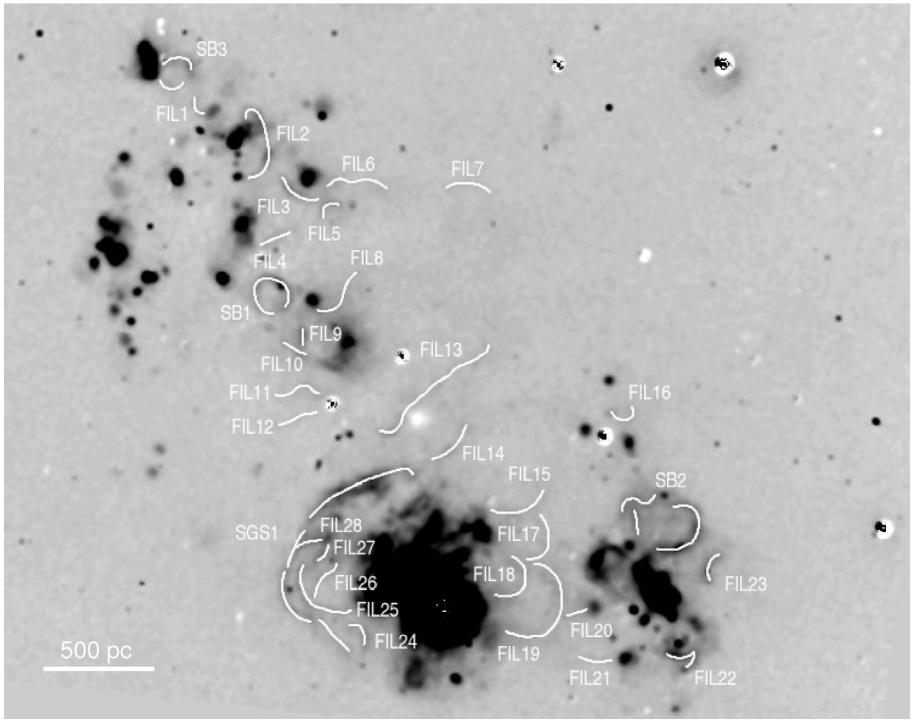

Fig. A.1. Continuum-subtracted Hα image of NGC 2366: position and designation of the filaments and shells are superimposed in white for better visibility. The contrast was chosen in a way to demonstrate the small scale structures. For a presentation of the large scale filaments see Fig. 2. A measure in pc to estimate the size of the structures is given in the lower left corner of the image. The distance of NGC 2366 is given in Table 1.

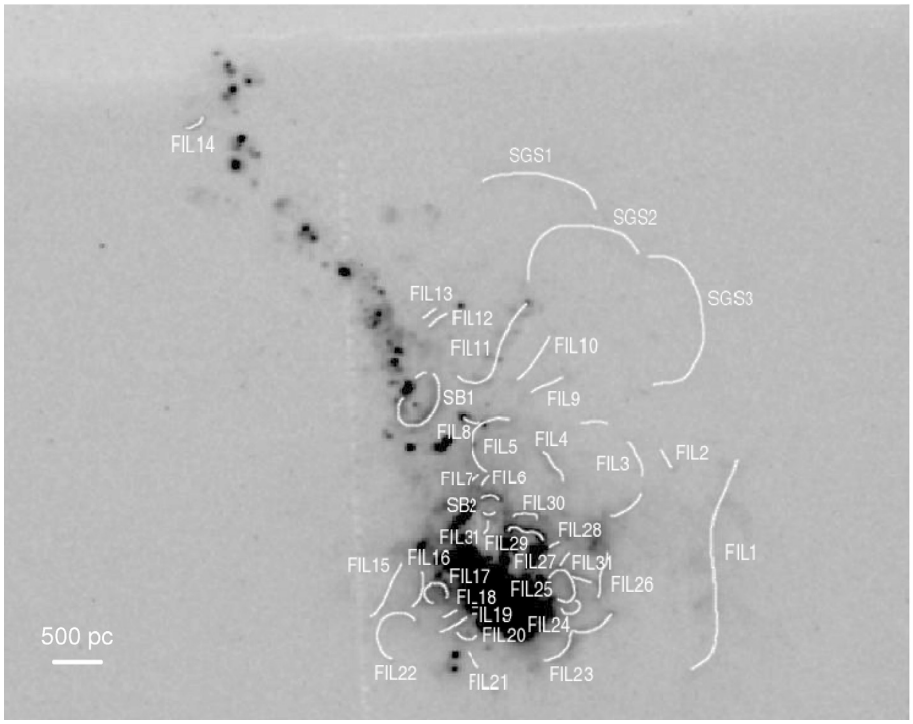

Fig. A.2. Continuum-subtracted Hα image of NGC 4861: position and designation of the filaments and shells are superimposed in white for better visibility. Again we chose a contrast for stressing the small scale structures. The large scale structure is shown in Fig. 3. To estimate the size of the structures, a measure in pc is given in the lower left corner of the image. The distance of NGC 4861 can be found in Table 1.

Appendix B: The echellograms

Figure B.1 shows the echellograms obtained with the KPNO 4 m telescope and its echelle spectrograph. The position with respect to the center of the GEHRs is drawn over the velocity with respect to the Hα line and corrected for the systemic velocity of the galaxies.

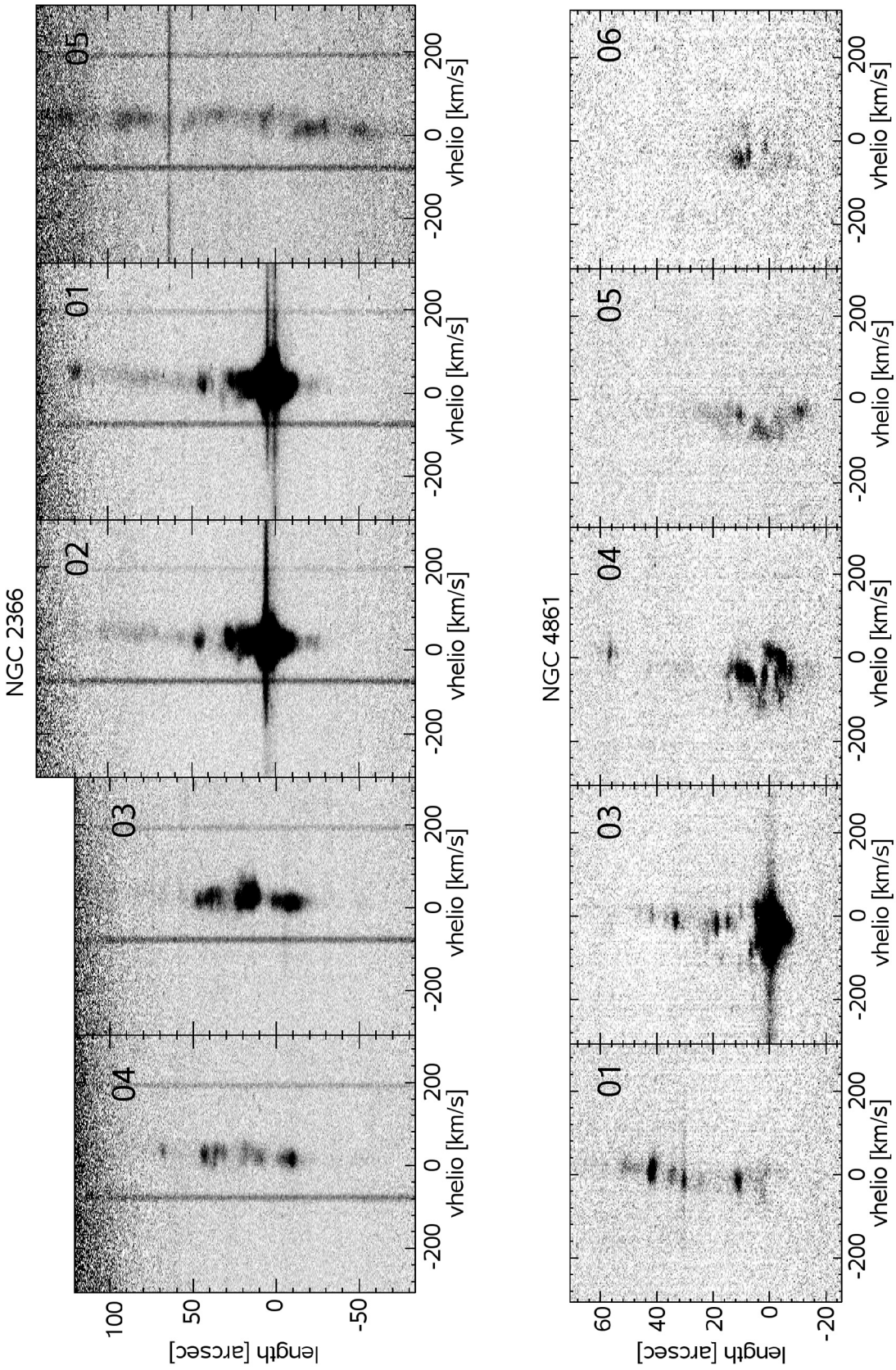

Fig. B.1. All echelle spectra of NGC 2366 and NGC 4861 arranged in a spatial sequence and centered on the Hα line which is corrected for the systemic velocity of each galaxy.